Article

TiO$_2$-Coated ZnO Nanowire Arrays: A Photocatalyst with Enhanced Chemical Corrosion Resistance

Lan Gao [1], Elyes Nefzaoui [1], Frédéric Marty [1], Mazen Erfan [1], Stéphane Bastide [2], Yamin Leprince-Wang [1,*] and Tarik Bourouina [1]

1   ESYCOM Lab, UMR 9007 CNRS, Université Gustave Eiffel, ESIEE Paris, 77454 Marne-la-Vallée, France; lan.gao@esiee.fr (L.G.); elyes.nefzaoui@esiee.fr (E.N.); frederic.marty@esiee.fr (F.M.); mazen.erfan@esiee.fr (M.E.); tarik.bourouina@esiee.fr (T.B.)
2   ICMPE, UMR 7182 CNRS, Université Paris Est Créteil, 2 Rue Henri Dunant, 94320 Thiais, France; bastide@icmpe.cnrs.fr
*   Correspondence: yamin.leprince@univ-eiffel.fr

Abstract: Photocatalysis is proven to be the most efficient and environmentally friendly method for the degradation of organic pollutants in water purification. To meet the requirement of large-scale water treatment, there are two important points: One is the lifetime and chemical stability of the photocatalyst material, especially in the complex and harsh aqueous conditions. The other is the ease of synthesis of such photocatalysts with specific nano-morphology. In this work, two common photocatalyst materials, zinc oxide (ZnO) and titanium dioxide (TiO$_2$), are selected to form more sustainable photocatalysts with high chemical stability. This involves the combination of both TiO$_2$ and ZnO in a two-step simple synthesis method. It appears advantageous to exploit the conformal deposition of atomic layer deposition (ALD) to achieve nanometer-thick TiO$_2$ coating on ZnO nanowires (NWs) with a high aspect ratio, which are firmly anchored to a substrate and exhibit a large specific surface area. The high chemical stability of the ALD TiO$_2$ coating has been investigated in detail and proven to be effective under both strong acid and strong alkaline aqueous solutions. In addition, photocatalysis experiments with organic dyes show that via this simple two-step synthesis method, the produced ZnO/TiO$_2$ tandem photocatalysts does indeed exhibit improved chemical stability in a harsh environment, while allowing efficient photodegradation.

Keywords: nanostructure; water purification; atomic layer deposition; ZnO nanowires; TiO$_2$ coating

1. Introduction

The combined effects of the growing human population, climate change, and increasing pollution are placing significant pressures on water resources. Water scarcity is steadily rising and has now become an urgent global issue. Thus, the development of new hygienically friendly water purification technologies has become urgent in order to ensure the sustainability of humanity's water supplies. One of the more sustainable solutions for water purification is the photocatalytic process, a non-selective organic pollutant degradation technique using solely solar energy and requiring a wide-bandgap semiconductor photocatalyst, such as ZnO [1,2] or TiO$_2$ [3,4], whose raw materials are abundant in nature and low-cost, and both have excellent photocatalytic properties. Both of these photocatalysts have been separately applied in water treatment research studies targeting wastewater with different organic pollutants [5,6]. However, in the real situation of water treatment, there are two main problems, resulting in the limitation of its development and large-scale application. One is the presence of an effluent that contains more complex pollutants and comprises a harsh aqueous condition, such as a strong acid or alkali solution environment. At the same time, the ease of synthesis of photocatalysts with a specific nano-morphology is another limitation for high-quality and large-scale water treatment applications.

The first problem has already been observed in many ZnO photocatalyst studies, wherein corrosion can cause damage to ZnO nanowires (NWs) during the photocatalysis process, thereby shortening their lifetime and decreasing device efficiency [7]. In addition, it has been reported that ZnO NWs can be damaged in harsh environments, such as in acidic or alkaline solutions [8]. In comparison, TiO_2 has a better corrosion resistance performance than ZnO, which is thus one possible solution for water treatment, especially in harsh conditions.

Another problem comes with the complicated synthesis of a specific nanostructured photocatalysts. Normally, to increase the contact opportunity between the photocatalyst and the organic pollutant molecules to enable their degradation, and thus improve the photocatalytic efficiency of the device, photocatalysts are often employed in nanostructured form, such as nanoparticles [9], nanorods [10], or nanowires [11]. Nanostructured photocatalysts can be used by direct dispersion in water, such as with a powder [12]. However, once the purification is complete, the separation of the photocatalytic particles and purified water is far from easy, and it often requires further filtration of the effluents, adding significant time and energy costs, and reducing the yield of the water treatment process. To avoid those additional steps, an alternative solution is to rely on a surface substrate supporting nanowire arrays with a high surface-to-volume ratio. This strategy has been frequently used and proven as an efficiency-enhanced photocatalyst [13]. Compared to TiO_2, whose NWs are usually synthesized in free form and dispersed in a growth solution, substrate-supported ZnO NW arrays can be easily synthesized onto a surface by chemical bath deposition such as a hydrothermal method. Such an alternative appears as a more environmentally friendly growth solution [14] and leads to ZnO NWs that are firmly anchored to the substrate, hence significantly reducing the risk of the detachment of the nanostructures to the surrounding environment. This is one of the reasons why ZnO NWs have drawn the attention of the research community, not only for their photocatalytic properties but also for their superior performances in different application fields, such as piezoelectric energy harvesting [15], photovoltaic solar cells [16], and chemical sensors [17,18].

Therefore, the targeted technical solution for effective water purification needs to simultaneously meet the following two conditions: (i) robust chemical resistance in the photocatalysts is needed to increase its lifetime; (ii) simple synthesis of the photocatalysts, which can be achieved on a solid substrate while maintaining a high surface-to-volume ratio, so as to achieve an effective chemical reaction rate. To meet all these requirements, a thin protective TiO_2 coating applied by atomic layer deposition onto the simple hydrothermally synthesized ZnO NWs could be straightforward, since atomic layer deposition (ALD) can produce conformal nanometer-thick coatings on all kinds of surfaces [19]. Several studies have reported that such an ALD TiO_2 coating can be successfully applied to ZnO nanoparticles [20,21] and ZnO nanocrystallite [22] for different applications, such as dye-sensitized solar cells [23] and solar-powered hydrogen gas harvesters [24]. For this reason, we expect a TiO_2/ZnO tandem photocatalyst to have robust chemical resistance under harsh conditions, while maintaining its high photocatalytic performance.

In this work, a TiO_2/ZnO tandem photocatalyst is used for its high aspect ratio, together with its considerable chemical stability under strong-pH aqueous conditions, which is crucial in water purification applications. The structure and morphology of the original ZnO NW samples with different TiO_2 coating thicknesses are compared before and after exposure to a solution with pH limit values, using high-resolution scanning electron microscopy (HR-SEM). The chemical compositions of the different TiO_2-ZnO tandems and their uniformity are assessed using energy-dispersive X-ray (EDX) analysis integrated into the HR-SEM system. Finally, the photodegradation of organic dye under UV light illumination using TiO_2-coated ZnO NWs is investigated for different TiO_2 coating thicknesses, with a focus on efficiency and chemical stability.

2. Results and Discussion

2.1. Characterization Results

After synthesis, EDX analysis was used to characterize ALD TiO_2-coated ZnO NW samples with different coating thicknesses, including 0 nm (bare ZnO NWs), 2 nm, 5 nm, and 10 nm. By focusing on a given position of the sample, the morphology and nanostructure as well as the composition of the sample can be obtained simultaneously at different positions. As shown in Figure 1, the EDX analysis with HR-SEM was carried out at three different positions on the ZnO NWs: bottom (●), middle (■), and top (▲). The observation points were 30 nm diameter spots on the sample's surface. By comparing the chemical composition at these three different heights, the conformity of the TiO_2 coating on ZnO NWs can be checked.
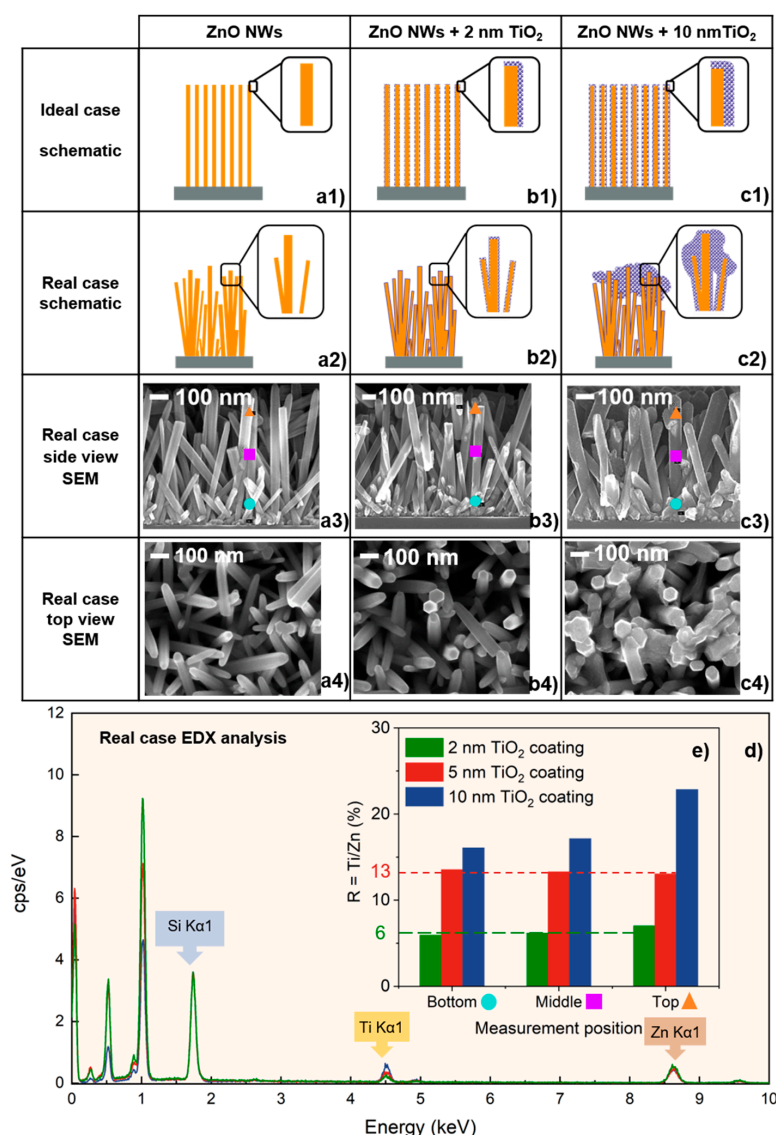
Figure 1. Characterization of TiO_2-coated ZnO NWs. (**a1,b1,c1**) Schematic descriptions of the ZnO NWs with TiO_2 coating in ideal cases with different thickness values and (**a2,b2,c2**) more realistic schematic descriptions. (**a3,b3,c3**) Cross-section SEM images showing the morphologies as well as the 3 different measurement positions from bottom to top. (**a4,b4,c4**) Top-view SEM images. (**d**) EDX spectra of the top position recorded on the 2 nm, 5 nm, and 10 nm TiO_2-coated ZnO NW samples. (**e**) The histogram of the Ti/Zn atomic ratio for different positions, bottom, middle, and top, on each of the 3 samples.

The schematic descriptions of the ZnO NWs with TiO_2 coating in ideal cases with different thickness values are shown in Figure 1a1,b1,c1. For each thickness of the coating, since the purpose of the ALD coating on ZnO NW is to obtain a uniform film, we expect that all samples cover with the same thickness from top to bottom. However, the SEM characterization showed slightly different results than expected. From the SEM images shown in Figure 1a3,b3,c3, one can clearly see that the average diameter of bare ZnO NW is about 40 ± 10 nm, and the width of ZnO NWs gradually increases as the TiO_2 coating thickness increases from 2 to 10 nm. A comparison with bare ZnO NWs shows that the 2 nm ALD TiO_2 coating maintains the NWs' high surface-to-volume ratio and good conformity. However, as the TiO_2 coating thickness increases, it starts accumulating at the top of the ZnO NWs. The schematic descriptions of more realistic cases are shown in Figure 1a2,b2,c2. In order to compare the conformity and quality of different ALD TiO_2 coatings, a coating coefficient R is defined in Equation (1), which is the ratio between the titanium and zinc atomic percentages for a given sample at a given position, where the titanium and zinc are provided by ALD TiO_2 coating and ZnO NWs, respectively. For example, when one measures the bare ZnO NWs, the value of R should be 0.

$$R = \frac{\text{number of Ti atoms}}{\text{number of Zn atoms}} \times 100\% \tag{1}$$

Then, the coating coefficient R is calculated at three different heights for all samples. The coating coefficient R of 2 nm and 5 nm TiO_2-coated ZnO NWs samples remains essentially unchanged from the bottom to the top position, at around 6.5 and 13, respectively. This shows that the ALD TiO_2 coatings cover the entire ZnO NW uniformly from bottom to top, as illustrated schematically in Figure 1a2,b2. The cross-section view SEM image of 5 nm TiO_2-coated ZnO NWs shows their very similar behavior to 2 nm TiO_2-coated ZnO NWs, which also indicates uniform coating (Figure S1, Supporting Information). When the coating thickness reaches 10 nm, the coating coefficient R from the bottom to the top is 16, 17, and 22, respectively. The R value at the top position is much larger than the R values at the middle and bottom, which confirms the morphological difference observed by HR-SEM of the sample shown in Figure 1c4. In addition, the EDX spectra of the samples with 2 nm, 5 nm and 10 nm TiO_2 coatings are also presented in Figure 1d. To avoid the confusion caused by other elements attached to the sample during the measurement process, the spectra were normalized and only compared with the K-line for quantifying Zn and Ti, instead of the L-line. Zn Kα and Ti Kα peaks were present at about 8.63 keV and 4.508 keV, respectively. At these two positions, one can clearly see that the quantity of the Ti increases as the coating thickness increases, while the quantity of the Zn remains the same. By comparing the R value shown in Figure 1e, we see that as the TiO_2 coating thickness increases, the ALD TiO_2 coating starts to accumulate on the top of the ZnO NWs, which also reduces the uniformity of the coating in the middle and bottom positions.

2.2. Stability in Harsh Chemical Conditions

After characterization, an experiment was conducted to evaluate the stability of the TiO_2/ZnO tandem photocatalysts under harsh aqueous conditions with different pH values. Sulfuric acid and sodium hydroxide were diluted in distilled (DI) water to prepare solutions from pH 3 to pH 11. Each sample was submitted to the pH solution bath for 30 min at room temperature and then rinsed with DI water three times to remove the residual pH solution. Severe damage was observed on a bare ZnO nanostructure at pH values lower than 4 and higher than 10. Thus, for the following study, pH 3 and pH 11 are chosen as harsh chemical conditions to compare the chemical corrosion resistance of bare ZnO NWs and TiO_2-coated ZnO NWs.

After exposure to the pH solution, SEM examination of each sample was carried out to compare the morphologies of samples with different TiO_2 coating thicknesses. The effect of the pH aqueous solution on TiO_2-coated ZnO NWs also has been tested from pH 3 to pH 11 (See details in Figure S2, Supporting Information). As shown in Figure 2a2,

significant damage to the nanostructure of bare ZnO NWs is observed after exposure to a pH 3 solution bath. With the increase in the ALD TiO$_2$ coating's thickness, there is an obvious protective effect. With a 2 nm TiO$_2$ coating, parts of the samples can survive the acid solution. For samples with 5 nm and 10 nm TiO$_2$ coating, this protective effect of the TiO$_2$ coating is steadily improved, and almost all samples can withstand a pH 3 solution bath. In the alkaline solution test, the sample was less affected and damaged than in the acidic solution, and even the exposed non-coated ZnO NWs maintained their pristine nanostructure after treatment in a solution at pH 11.
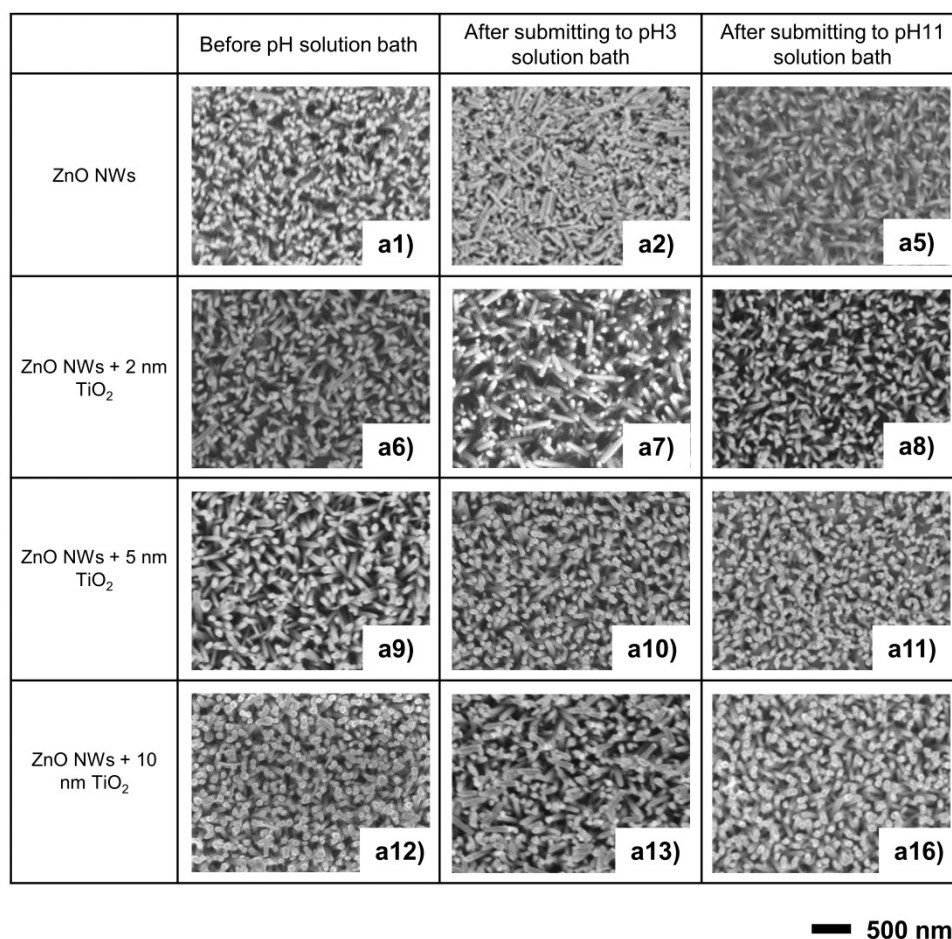

Figure 2. SEM images of the effect of TiO$_2$ coating thickness on ZnO NWs in strong acid/alkaline aqueous solutions.

In Figure 3a–c, three SEM images of the same sample under different magnifications are shown along with a schematic to illustrate the protective effect of the ALD TiO$_2$ coating on ZnO NWs. The whole sequence illustrates what happens in a specific region of the sample that is exposed to mechanical damage (Figure 3d). In those specific damaged regions only, the NWs are broken, and consequently, there is no more protective TiO$_2$ coating on the topmost part of the broken NWs. This lack of protective TiO$_2$ coating caused the ZnO NWs to react with the acid solution, eventually resulting in the complete dissolution of the ZnO NWs' core. Only the ALD TiO$_2$ shells were left, which appear translucent on the left side of Figure 3c. In contrast, in the absence of mechanical damage (right side of Figure 3c and other regions of the sample, except those with stripes), all the ZnO NWs protected by a fully conformal coating remained intact, and appear opaque in the SEM image.
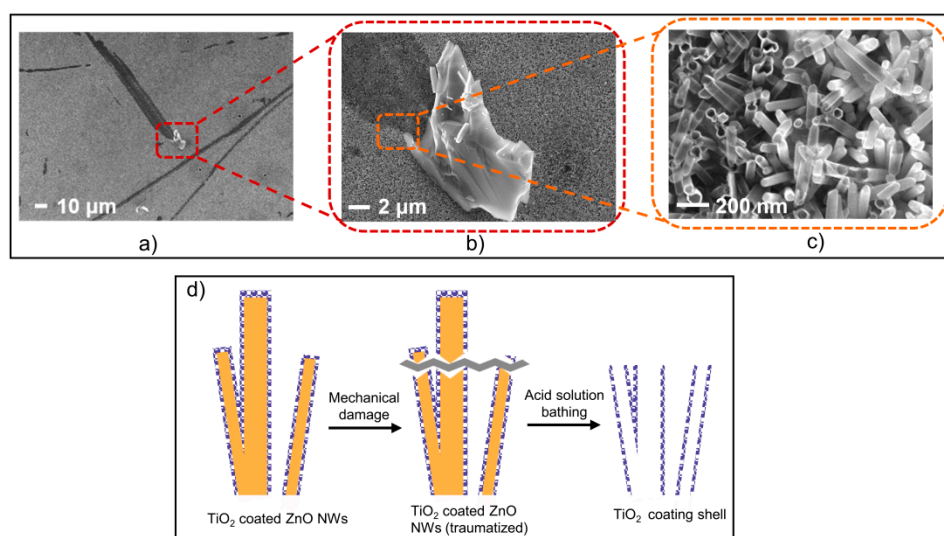
Figure 3. (**a**–**c**) Zoomed SEM views of 10 nm ALD TiO$_2$ coating on ZnO NWs after bathing in pH 3 aqueous solution for 30 min. (**d**) A schematic of the protective effect of the TiO$_2$ coating.

2.3. Photodegradation of Organic Dye for Water Purification

UV-Vis spectroscopy was used to evaluate the photodegradation efficiency of the organic dye MB (Certistain®, SigmaAldrich, Burlington, MA, USA), which is one of the most common pollutants in industrial wastewater [25], and the process of the photodegradation experiment was basically the same as in our previous research [26,27]. The evolution of the MB concentration has been assessed by absorption spectroscopy at 665 nm, corresponding to the strongest absorption peak. The photodegradation efficiency at each sampling time is expressed by Equation (2):

$$\eta = \left| \frac{A_0 - A_t}{A_0} \right| \times 100\% \tag{2}$$

where A_0 and A_t are the intensities of the absorption peaks of the original solution and the treated solution (in arbitrary units) after UV exposure, and the photocatalysis process was suspended during the sampling. The recorded spectra are given in Figure S3 of the Supporting Information.

As shown in Figure 4a, the best photodegradation efficiency of MB was obtained with samples of bare ZnO NWs. Almost 100% degradation was achieved using such bare ZnO NWs in less than 120 min, while the samples with TiO$_2$ ALD coatings showed slower degradation kinetics and required longer reaction times to achieve the 100% degradation of MB. To evaluate the kinetic degradation loss, a characteristic time constant τ has been defined, as the time needed to achieve 63.2% degradation efficiency ($\eta = 1 - 1/e$). As the thickness of the TiO$_2$ coating on the ZnO NWs increased from 0 (bare ZnO NWs) to 10 nm, the characteristic time constant τ also increased, to values of 43, 83, 106, and 91 min, respectively. This indicates that the ALD TiO$_2$ coating on ZnO NWs is very useful for ensuring chemical robustness; it also has the side effect of weakening and limiting the degradation process.
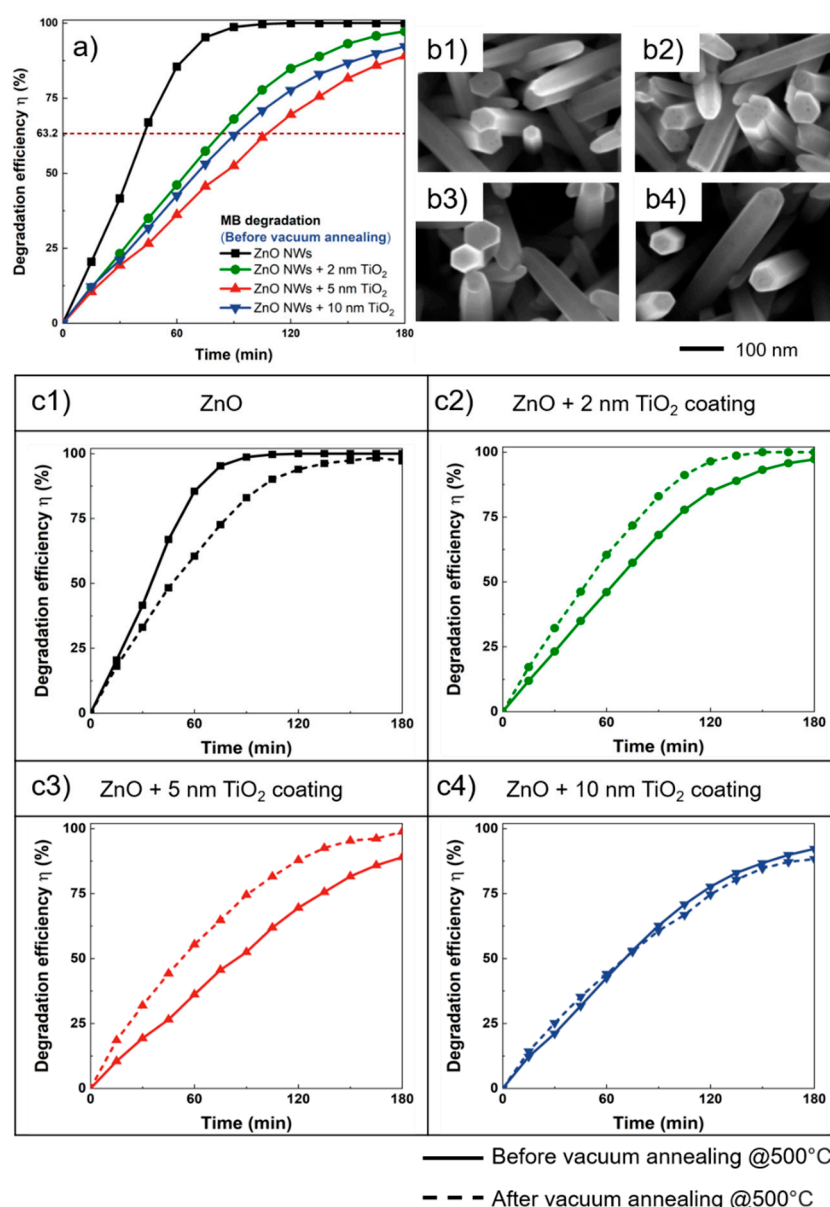
Figure 4. (**a**) Comparison of the photodegradation efficiency of MB among the different TiO_2 coating thicknesses from 0 to 10 nm. (**b**) The SEM photos of the ZnO NWs before (**b1**) and after vacuum-annealing (**b2**), 2 nm TiO_2-coated ZnO NWs before (**b3**) and after vacuum-annealing (**b4**). (**c1–c4**) Comparison of photodegradation efficiency of different samples before and after vacuum-annealing.

In fact, the catalytic activity of ZnO catalysts is slightly higher than that of TiO_2. Even though the bandgaps of titanium and zinc oxide are very similar, the mobility of the charge carriers of ZnO is higher (by a factor of 100) than that of TiO_2 [28,29]. At the same time, the decreasing of the effective surface-to-volume ratio could also be another reason behind the reduction in TiO_2-coated ZnO photodegradation efficiency. In addition, the formation of the ZnO-TiO_2 interface may prevent the separation of charge carriers, thereby increasing the electron–hole recombination rate and hence affecting the photocatalytic activity. However, as the thickness of the ALD increased, the photodegradation efficiency was shown to exhibit a slight increase. This can be explained as TiO_2 is another well-known photocatalysis material that also contributes to the degradation of the MB. The band gap measurements of the samples also confirm the contribution of the 10 nm TiO_2 coating to ZnO NWs (Figure S4, Supporting Information). In fact, the results show that the band gaps

of the ZnO NWs, as well as the 2 nm and 5 nm TiO_2-coated ZnO NWs, remained almost unchanged, at around 3.18 eV, whereas the band gaps of the 10 nm TiO_2-coated ZnO NWs were around 3.21 eV. After 180 min of reaction, the degradation rate of MB reached 100%, 97.24%, 89.02%, and 92.20% for 0 nm, 2 nm, 5 nm, and 10 nm, respectively.

Since the ALD TiO_2-coated ZnO NWs have some weakening effect on the degradation efficiency, we explored another strategy to further increase the photodegradation efficiency of the TiO_2-coated ZnO NWs. It has been already proven that in the photocatalysis process, oxygen vacancies can be used as important adsorption and active sites, thereby affecting the efficiency of photodegradation [30]. Depending on the different methods, the oxygen vacancies formed at different positions have different effects on electric charge separation [31,32]. Considering that the photocatalysis degradation is almost entirely a surface chemical reaction process, annealing at 500 °C under vacuum for 1 h was applied to the samples in order to increase the surface oxygen vacancy. From Figure 4b1,b2, compared with before vacuum-annealing, increases in the tiny pore structure of the exposed ZnO nanowires can be observed, and these are probably formed by the oxygen vacancy under the vacuum conditions. However, when vacuum-annealing was applied to the 2 nm TiO_2-coated ZnO NWs samples, as shown in Figure 4b3,b4, there is no obvious increase in the tiny pore structure of the samples. In Figure 4c, one can see the photodegradation efficiency of the samples with different TiO_2 coating thicknesses before and after annealing. The ZnO NWs samples coated with 2 nm and 5 nm TiO_2 exhibit better photodegradation efficiencies after annealing, of 100% and 98.83%. In order to evaluate the formation of defects in the sample, the photoluminescence spectrum was recorded before and after vacuum-annealing (Figure S5, Supporting Information), which shows a good agreement with the increase in oxygen vacancy defects benefiting from the vacuum-annealing process. The introduction of surface oxygen vacancies can not only form a defect state under the conduction band of the photocatalyst to reduce the bandgap and increase the absorption of visible light, but it can also serve as a trapping center for photogenerated electrons in order to inhibit the recombination of photogenerated electron–hole pairs, thereby improving the photocatalytic [33]. For the bare ZnO NWs sample, the dynamic degradation efficiency was slightly lower than previously. This difference might be due to the different processes of oxygen vacancy formation. When the concentration of oxygen vacancies is greater than a given threshold, the oxygen vacancies behave as charge recombination centers, and reduce the mobility of free charges and photocatalytic activity [34].

3. Experimental Section

3.1. Sample Fabrication and pH Solution Preparation

All the photocatalyst samples were synthesized in a simple 2-step method. Firstly, the ZnO NWs samples were prepared via a hydrothermal synthesis method slightly adapted from our previous works [14].

Then, a uniform and conformal coating of TiO_2 can be deposited on the ZnO samples via a precise chemical vapor deposition process at 300 °C. A first titanium tetrachloride ($TiCl_4$) precursor was injected into the reactor for 0.2 s. This was intended to be adsorbed by the sample's surface until saturation. Then, the reactor was purged with nitrogen (N_2) gas long enough to remove any trace of titanium tetrachloride. A purge duration of 6 s was used. Next, water was injected into the reactor for 0.2 s to start the self-limiting reaction with the titanium tetrachloride. Finally, the reactor was purged again with nitrogen for 6 s to finish the first deposition cycle. This cycle was repeated to reach the targeted TiO_2 thickness. The sample information is listed in Table 1.

To test the protective effect of the ALD TiO_2 coating in both acid and alkaline aqueous environments, a series of aqueous solutions with different pH values was prepared to simulate harsh aqueous conditions. Sulfuric acid and sodium hydroxide were diluted into the DI water to prepare solutions with different pH values from pH 3 to pH 11. Each sample was submitted to the pH solution bath for 30 min at room temperature and then rinsed with DI water three times to remove the residual pH solution.

Table 1. Sample information.

Sample ID	Sample Content	pH Solution Treatment
a1	ZnO NWs	No treatment
a2	ZnO NWs	pH 3
a3	ZnO NWs	pH 5
a4	ZnO NWs	pH 9
a5	ZnO NWs	pH 11
a6	ZnO NWs + 2 nm ALD TiO_2	No treatment
a7	ZnO NWs + 2 nm ALD TiO_2	pH 3
a8	ZnO NWs + 2 nm ALD TiO_2	pH 11
a9	ZnO NWs + 5 nm ALD TiO_2	No treatment
a10	ZnO NWs + 5 nm ALD TiO_2	pH 3
a11	ZnO NWs + 5 nm ALD TiO_2	pH 11
a12	ZnO NWs + 10 nm ALD TiO_2	No treatment
a13	ZnO NWs + 10 nm ALD TiO_2	pH 3
a14	ZnO NWs + 10 nm ALD TiO_2	pH 5
a15	ZnO NWs + 10 nm ALD TiO_2	pH 9
a16	ZnO NWs + 10 nm ALD TiO_2	pH 11

3.2. Characterization and Photodegradation Experiment

For characterization, EDX analysis (HR-SEM) was used to characterize ALD TiO_2-coated ZnO NW samples using a Zeiss Merlin Field Emission Scanning Electron Microscope operating at 5 kV (Oberkochen, Germany).

For the photodegradation experiment, MB (methylene blue) was dissolved in deionized water at a concentration of 10 μmol L^{-1}. The dye solution was then placed beneath a UV light (Hamamatsu LC8, Janpan, 4500 mW/cm^2, λ = 365 nm) with a vertical incidence, and the distance between the surface of the solution and the light source was 10 cm; therefore, the received irradiation on the solution surface was about 35 mW/cm^2, measured by a UV light meter (Lutron, Taiwan, UV-340A). Photodegradation was carried out in dynamic mode, i.e., under slight magnetic stirring to enhance the mass transport in the solution [27]. The photodegradation efficiency was recorded via the decrease in the absorbance of the solution over time, which was measured via UV-Vis spectroscopy (Lambda 35, Perkin Elmer, Waltham, MA, USA).

4. Conclusions

In summary, an investigation is reported on a simple two-step synthesis method that can provide high-aspect ratio TiO_2/ZnO tandem photocatalysts, with the aim of enhancing their lifetime and chemical stability under harsh aqueous solution pH conditions, with applications mainly in water purification. It is demonstrated that the ALD TiO_2 coating offers a sustainable protective layer thanks to its good conformity on the ZnO NWs' surface, even with a thin TiO_2 coating. With the help of EDX analysis via HR-SEM measurements, this study also revealed that as the coating thickness increases, the coating starts to accumulate on the top surface of the ZnO NWs, which limits the conformal coating on the middle and bottom positions, leading to an optimal value of around 5 nm for the TiO_2 coating. There is no doubt that even for pH 3 solutions, the ALD TiO_2 coating has a significant protective effect on ZnO NWs; in particular, when there are no mechanical defects in the coating, the protected ZnO NWs remain intact. The photodegradation efficiency of different thicknesses of TiO_2-coated ZnO NWs has also been tested, whereby the TiO_2-coated ZnO NWs were shown to undergo a slight reduction when the TiO_2 coating thickness increased, compared to bare ZnO NWs. We finally proved that this degradation efficiency reduction can be minimized by simple vacuumannealing. Although more research is needed to reveal the photocatalytic mechanism of TiO_2-coated ZnO NWs, our findings will provide a good reference for researchers interested in using ZnO NWs for practical applications.

Author Contributions: Y.L.-W. and T.B. devised the project, the main conceptual ideas and proof outline. L.G. is the main contributor to this study as part of her Ph.D. work. L.G. conducted the experiments of ZnO NWs growth and photodegradation. F.M. contributed to atomic layer deposition layer fabrication. S.B. and M.E. characterized the samples with energy-dispersive X-ray (EDX) analysis-integrated high-resolution scanning electron microscopy. E.N. contributed to the reviewing of the manuscript. All authors have read and agreed to the published version of the manuscript.

Conflicts of Interest: The authors declare no conflict of interest.

References

1. Qin, H.; Li, W.; Xia, Y.; He, T. Photocatalytic Activity of Heterostructures Based on ZnO and N-Doped ZnO. *ACS Appl. Mater. Interfaces* **2011**, *3*, 3152–3156. [CrossRef]

2. Hariharan, C. Photocatalytic Degradation of Organic Contaminants in Water by ZnO Nanoparticles: Revisited. *Appl. Catal. A Gen.* **2006**, *304*, 55–61. [CrossRef]

3. Shayegan, Z.; Lee, C.-S.; Haghighat, F. TiO$_2$ Photocatalyst for Removal of Volatile Organic Compounds in Gas Phase–A Review. *Chem. Eng. J.* **2018**, *334*, 2408–2439. [CrossRef]

4. Konstantinou, I.K.; Albanis, T.A. TiO$_2$-Assisted Photocatalytic Degradation of Azo Dyes in Aqueous Solution: Kinetic and Mechanistic Investigations: A Review. *Appl. Catal. B Environ.* **2004**, *49*, 1–14. [CrossRef]

5. Roy, N.; Chakraborty, S. ZnO as Photocatalyst: An Approach to Waste Water Treatment. *Mater. Today Proc.* **2021**, *46*, 6399–6403. [CrossRef]

6. Fiorenza, R.; Bellardita, M.; Scirè, S.; Palmisano, L. Photocatalytic H$_2$ Production over Inverse Opal TiO$_2$ Catalysts. *Catal. Today* **2019**, *321*, 113–119. [CrossRef]

7. Spathis, P.; Poulios, I. The Corrosion and Photocorrosion of Zinc and Zinc Oxide Coatings. *Corros. Sci.* **1995**, *37*, 673–680. [CrossRef]

8. Zhou, J.; Xu, N.S.; Wang, Z.L. Dissolving Behavior and Stability of ZnO Wires in Biofluids: A Study on Biodegradability and Biocompatibility of ZnO Nanostructures. *Adv. Mater.* **2006**, *18*, 2432–2435. [CrossRef]

9. Hong, R.Y.; Li, J.H.; Chen, L.L.; Liu, D.Q.; Li, H.Z.; Zheng, Y.; Ding, J. Synthesis, Surface Modification and Photocatalytic Property of ZnO Nanoparticles. *Powder Technol.* **2009**, *189*, 426–432. [CrossRef]

10. Ren, C.; Yang, B.; Wu, M.; Xu, J.; Fu, Z.; Guo, T.; Zhao, Y.; Zhu, C. Synthesis of Ag/ZnO Nanorods Array with Enhanced Photocatalytic Performance. *J. Hazard. Mater.* **2010**, *182*, 123–129. [CrossRef]

11. Kuo, T.-J.; Lin, C.-N.; Kuo, C.-L.; Huang, M.H. Growth of Ultralong ZnO Nanowires on Silicon Substrates by Vapor Transport and Their Use as Recyclable Photocatalysts. *Chem. Mater.* **2007**, *19*, 5143–5147. [CrossRef]

12. Youssef, Z.; Colombeau, L.; Yesmurzayeva, N.; Baros, F.; Vanderesse, R.; Hamieh, T.; Toufaily, J.; Frochot, C.; Roques-Carmes, T.; Acherar, S. Dye-Sensitized Nanoparticles for Heterogeneous Photocatalysis: Cases Studies with TiO$_2$, ZnO, Fullerene and Graphene for Water Purification. *Dye. Pigment.* **2018**, *159*, 49–71. [CrossRef]

13. Le Pivert, M.; Zerelli, B.; Martin, N.; Capochichi-Gnambodoe, M.; Leprince-Wang, Y. Smart ZnO Decorated Optimized Engineering Materials for Water Purification under Natural Sunlight. *Constr. Build. Mater.* **2020**, *257*, 119592. [CrossRef]

14. Chevalier-César, C.; Capochichi-Gnambodoe, M.; Leprince-Wang, Y. Growth Mechanism Studies of ZnO Nanowire Arrays via Hydrothermal Method. *Appl. Phys. A* **2014**, *115*, 953–960. [CrossRef]

15. Leprince-Wang, Y. *Piezoelectric ZnO Nanostructure for Energy Harvesting*; John Wiley & Sons: London, UK, 2015; Volume 1.

16. Kao, M.-C.; Chen, H.-Z.; Young, S.-L.; Lin, C.-C.; Kung, C.-Y. Structure and Photovoltaic Properties of ZnO Nanowire for Dye-Sensitized Solar Cells. *Nanoscale Res. Lett.* **2012**, *7*, 260. [CrossRef] [PubMed]

17. Fathy, A.; Le Pivert, M.; Kim, Y.J.; Ba, M.O.; Erfan, M.; Sabry, Y.M.; Khalil, D.; Leprince-Wang, Y.; Bourouina, T.; Gnambodoe-Capochichi, M. Continuous Monitoring of Air Purification: A Study on Volatile Organic Compounds in a Gas Cell. *Sensors* **2020**, *20*, 934. [CrossRef] [PubMed]

18. Umar, A.; Rahman, M.M.; Hahn, Y.-B. Ultra-Sensitive Hydrazine Chemical Sensor Based on High-Aspect-Ratio ZnO Nanowires. *Talanta* **2009**, *77*, 1376–1380. [CrossRef] [PubMed]

19. Knez, M.; Nielsch, K.; Niinistö, L. Synthesis and Surface Engineering of Complex Nanostructures by Atomic Layer Deposition. *Adv. Mater.* **2007**, *19*, 3425–3438. [CrossRef]

20. Sridharan, K.; Jang, E.; Park, Y.M.; Park, T.J. Superior Photostability and Photocatalytic Activity of ZnO Nanoparticles Coated with Ultrathin TiO_2 Layers through Atomic-Layer Deposition. *Chem.–A Eur. J.* **2015**, *21*, 19136–19141. [CrossRef]

21. Mousa, H.M.; Alenezi, J.F.; Mohamed, I.M.; Yasin, A.S.; Hashem, A.-F.M.; Abdal-hay, A. Synthesis of TiO_2@ZnO Heterojunction for Dye Photodegradation and Wastewater Treatment. *J. Alloys Compd.* **2021**, *886*, 161169. [CrossRef]

22. Park, K.; Zhang, Q.; Garcia, B.B.; Zhou, X.; Jeong, Y.-H.; Cao, G. Effect of an Ultrathin TiO_2 Layer Coated on Submicrometer-Sized ZnO Nanocrystallite Aggregates by Atomic Layer Deposition on the Performance of Dye-Sensitized Solar Cells. *Adv. Mater.* **2010**, *22*, 2329–2332. [CrossRef]

23. Chandiran, A.K.; Abdi-Jalebi, M.; Nazeeruddin, M.K.; Grätzel, M. Analysis of Electron Transfer Properties of ZnO and TiO_2 Photoanodes for Dye-Sensitized Solar Cells. *ACS Nano* **2014**, *8*, 2261–2268. [CrossRef] [PubMed]

24. Kao, E.; Park, H.S.; Zang, X.; Lin, L. Atomic Layer Deposition of TiO_2 Nanocoatings on ZnO Nanowires for Improved Photocatalytic Stability. *Int. J. Photoenergy* **2019**, *2019*, 8982672. [CrossRef]

25. Leprince-Wang, Y.; Martin, N.; Habba, Y.G.; Le Pivert, M.; Capochichi-Gnambodoe, M. ZnO Nanostructure Based Photocatalysis for Water Purification. *NanoWorld J.* **2020**, *6*, 1–6. [CrossRef]

26. Houas, A.; Lachheb, H.; Ksibi, M.; Elaloui, E.; Guillard, C.; Herrmann, J.-M. Photocatalytic Degradation Pathway of Methylene Blue in Water. *Appl. Catal. B Environ.* **2001**, *31*, 145–157. [CrossRef]

27. Habba, Y.G.; Capochichi-Gnambodoe, M.; Leprince-Wang, Y. Enhanced Photocatalytic Activity of Iron-Doped ZnO Nanowires for Water Purification. *Appl. Sci.* **2017**, *7*, 1185. [CrossRef]

28. Janisch, R.; Gopal, P.; Spaldin, N.A. Transition Metal-Doped TiO_2 and ZnO—Present Status of the Field. *J. Phys. Condens. Matter* **2005**, *17*, R657. [CrossRef]

29. Quintana, M.; Edvinsson, T.; Hagfeldt, A.; Boschloo, G. Comparison of Dye-Sensitized ZnO and TiO_2 Solar Cells: Studies of Charge Transport and Carrier Lifetime. *J. Phys. Chem. C* **2007**, *111*, 1035–1041. [CrossRef]

30. Pan, X.; Yang, M.-Q.; Fu, X.; Zhang, N.; Xu, Y.-J. Defective TiO_2 with Oxygen Vacancies: Synthesis, Properties and Photocatalytic Applications. *Nanoscale* **2013**, *5*, 3601–3614. [CrossRef]

31. Gonullu, M.P.; Ates, H. Investigation of the Impact of Annealing on the Structural, Optical and Morphological Evolution of Mixture-Phase ALD-TiO_2 Films Containing Brookite. *Superlattices Microstruct.* **2020**, *147*, 106699. [CrossRef]

32. Won, S.; Go, S.; Lee, W.; Jeong, K.; Jung, H.; Lee, C.; Lee, E.; Lee, J. Effects of Defects Generated in ALD TiO_2 Films on Electrical Properties and Interfacial Reaction in $TiO_2/SiO_2/Si$ System upon Annealing in Vacuum. *Met. Mater. Int.* **2008**, *14*, 759–765. [CrossRef]

33. Huygh, S.; Bogaerts, A.; Neyts, E.C. How Oxygen Vacancies Activate CO_2 Dissociation on TiO_2 Anatase (001). *J. Phys. Chem. C* **2016**, *120*, 21659–21669. [CrossRef]

34. Tan, H.; Zhao, Z.; Zhu, W.; Coker, E.N.; Li, B.; Zheng, M.; Yu, W.; Fan, H.; Sun, Z. Oxygen Vacancy Enhanced Photocatalytic Activity of Pervoskite $SrTiO_3$. *ACS Appl. Mater. Interfaces* **2014**, *6*, 19184–19190. [CrossRef] [PubMed]